Modelling of effects of nose radomes on radar antenna performance

CUSTOMER: Netherlands Aerospace Centre

NLR – Netherlands Aerospace Centre

nlr Dedicated to innovation in aerospace
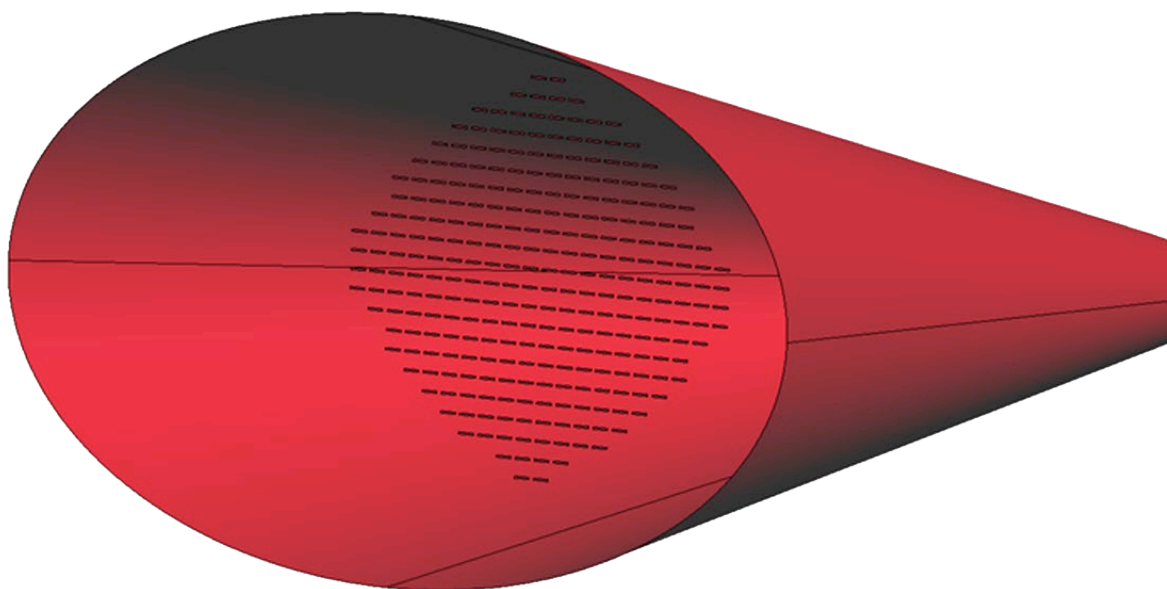
Netherlands Aerospace Centre

NLR is a leading international research centre for aerospace. Bolstered by its multidisciplinary expertise and unrivalled research facilities, NLR provides innovative and integral solutions for the complex challenges in the aerospace sector.

NLR's activities span the full spectrum of Research Development Test & Evaluation (RDT & E). Given NLR's specialist knowledge and facilities, companies turn to NLR for validation, verification, qualification, simulation and evaluation. NLR thereby bridges the gap between research and practical applications, while working for both government and industry at home and abroad.

NLR stands for practical and innovative solutions, technical expertise and a long-term design vision. This allows NLR's cutting edge technology to find its way into successful aerospace programs of OEMs, including Airbus, Embraer and Pilatus. NLR contributes to (military) programs, such as ESA's IXV re-entry vehicle, the F-35, the Apache helicopter, and European programs, including SESAR and Clean Sky 2.

Founded in 1919, and employing some 650 people, NLR achieved a turnover of 71 million euros in 2016, of which three-quarters derived from contract research, and the remaining from government funds.

For more information visit: **www.nlr.nl**

Modelling of effects of nose radomes on radar antenna performance
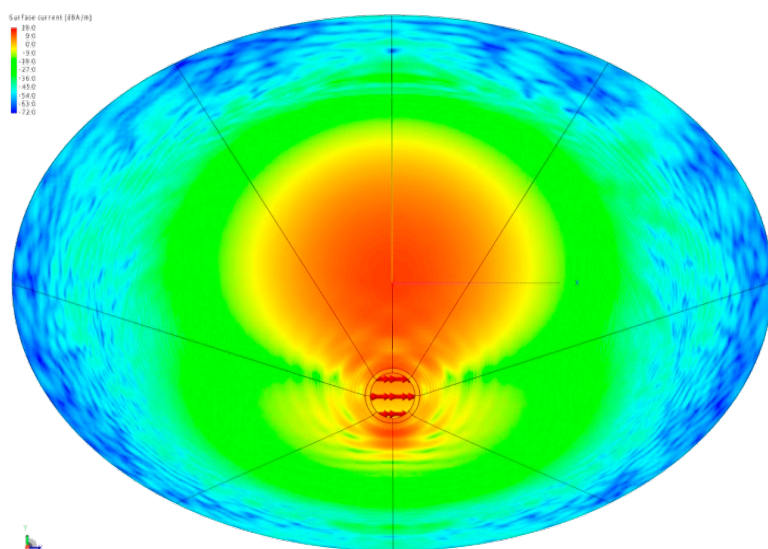
Problem area

Both military and civil aircraft are usually equipped with nose radomes to protect their radar antennas against rain, wind and for instance bird impact. These radomes affect the radiation pattern of the antenna, since they are never entirely transparent for electromagnetic waves. Moreover, the radomes may comprise inhomogeneities like lightning diverters and tuning tapes. Effects of nose radomes can be observed in attenuation and deflection of the antenna's main lobe, as well as reflection lobes. Knowledge about the effects of various radomes and their inhomogeneities can be obtained by computer simulations. If such simulations are computationally efficient, they can assist in procedures to optimise transmission through radomes.

Description of work

This paper presents an improved Physical Optics (PO) method, with which the radiation pattern of the combined nose radome and radar antenna can be analysed. The method takes into account the thickness and material properties of the radome, and can be applied to radomes with multiple layers (including for instance coating). Apart from the PO method, two implementations of the full-wave Multi-Level Fast Multipole Algorithm (MLFMA) are discussed. The improved PO and these two implementations of the MLFMA are applied to a generic radar antenna covered by a generic radome. Results of the three methods are compared for a code-to-code validation. Finally, the PO and an NLR in-house MLFMA implementation are also applied to an available fighter-like radome and antenna.

Results and conclusions

The three different simulation methods lead to comparable results when applied to the generic radome and radar antenna. Especially with respect to important properties of the radar antenna pattern, such as main beam attenuation and deflection, as well as the position of the reflection lobe, the accuracy is good. Differences between the PO and MLFMA codes arise from the absence of multiple reflections in the high-frequency PO method. These are taken into account in the MLFMA. The single reflection in the PO method causes a slight overestimation of the reflection lobe. However, for the improved PO the computational effort and resources that are required are much lower than for the MLFMA.

Applicability

The thickness of nose radomes may be optimised to achieve optimal transmission of radar energy. To this extent, locally the thickness of radomes can be tuned by the use of tuning tapes. The developed improved Physical Optics tool can be used to investigate the effect of nose radomes and corresponding inhomogeneities on the antenna pattern, but also to assist in tuning procedures.

Modelling of effects of nose radomes on radar antenna performance

AUTHOR(S):

J.H.G.J. Lansink Rotgerink	NLR
H. van der Ven	NLR
T. Voigt	Altair Engineering GmbH
E. Jehamy	Altair Engineering GmbH
M. Schick	Altair Engineering GmbH
H. Schippers	NLR

NLR - Netherlands Aerospace Centre

CUSTOMER	Netherlands Aerospace Centre
CONTRACT NUMBER	-----
OWNER	NLR
DIVISION NLR	Aerospace Systems
DISTRIBUTION	Unlimited
CLASSIFICATION OF TITLE	UNCLASSIFIED

APPROVED BY :

AUTHOR	REVIEWER	MANAGING DEPARTMENT
J.H.G.J. Lansink Rotgerink	J.J.P. van Es	M. Keuning
DATE 0 6 0 4 1 8	DATE 0 3 0 4 1 8	DATE 1 6 0 4 1 8

Contents

This page is intentionally left blank.

Modelling of effects of nose radomes on radar antenna performance

J. Lansink Rotgerink[1], H. van der Ven[2], T. Voigt[3], E. Jehamy[4], M. Schick[5], H. Schippers[6]

[1] Aerospace Systems Division, Netherlands Aerospace Centre, Marknesse, The Netherlands, Jesper.Lansink.Rotgerink@nlr.nl

[2] Aerospace Vehicles Division, Netherlands Aerospace Centre, Amsterdam, The Netherlands, Harmen.van.der.Ven@nlr.nl

[3] Altair Engineering GmbH, Böblingen, Germany, voigt@altair.de

[4] Altair Engineering GmbH, Lyon, France, ejehamy@altair.com

[5] Altair Engineering GmbH, Böblingen, Germany, schick@altair.de

[6] Aerospace Systems Division, Netherlands Aerospace Centre, Marknesse, The Netherlands, Harmen.Schippers@nlr.nl

Abstract—**This paper describes two computational models for the assessment of effects of nose radomes on the performance of radar antennas. The first model is an improved Physical Optics approach that takes into account the wall thickness and multiple layers of the radome. The second model follows from the accelerated numerical solution of Electric Field and Magnetic Field Integral equations. The models are applied to predict the radiation patterns of a radar antenna behind a generic nose radome and behind a radome of a fighter aircraft. The applicability of the two models is discussed.**

Index Terms—**antenna, propagation, radome, radar, numerical simulation, physical optics, method of moments, scattered fields.**

I. INTRODUCTION

Military and civil aircraft are usually equipped with nose radomes to protect weather and radar antennas from rain and wind. The presence of such a radome affects the antenna pattern of the radar antenna. This leads to deflection, reflection and attenuation of the principal beam of the radar antenna. Moreover due to reflections image lobes can occur in the radiation pattern. There exist specific requirements for acceptance for all these errors, since it can cause for instance false targeting. To achieve optimum transmission through the radome the local thickness needs to be optimised taking into account the applied materials inside the radome wall. To this end radomes need to be tuned with respect to the thickness. In practice, this is realised by locally adding dielectric tuning tapes to the interior side of the radome. Knowledge about positioning of tuning tapes can be obtained by successive computer simulations within acceptable computational time.

For the electromagnetic analysis of nose radomes several computational methods are available. These methods can be subdivided into two categories: Approximate High-Frequency (HF) methods based on ray tracing techniques combined with physical optics and full-wave solvers which solve the Maxwell equations or Stratton-Chu integral equations more accurately by means of Finite Element Methods (FEM) or Method of Moments. The surface of the radome of a fighter aircraft is large in terms of square wavelength (the fighter-like radome analysed in this paper is about $3400\lambda^2$, with λ the wavelength of the X-band radar antenna). Therefore the electromagnetic analysis is characterized as high-frequent. Computational methods require that the surface of a nose radome is divided into triangular or quadrilateral elements. On each element the variation of the phase of the electromagnetic waves needs to be modelled in a sufficiently accurate way. In case the phase is taken constant over a single element, the sizes of edges of triangular or quadrilateral elements should not be larger than $\lambda/7$. For the surface of a fighter-like radome this implies necessity for about 333200 triangular elements. The required computational resources for HF methods are of $O(N)$ with N the number of triangular elements. For the classical Methods of Moments (MoM) the required computational resources are $O(N^3)$. Hence the application of MoM to nose radomes of typical fighters leads to extensive computations. Much research was performed to reduce the computational resources of MoM by the introduction of novel techniques such as Fast Multipole expansions and Multi-level schemes. These novel techniques reduce the required computational resources of MoM type methods to $O(N\log N)$.
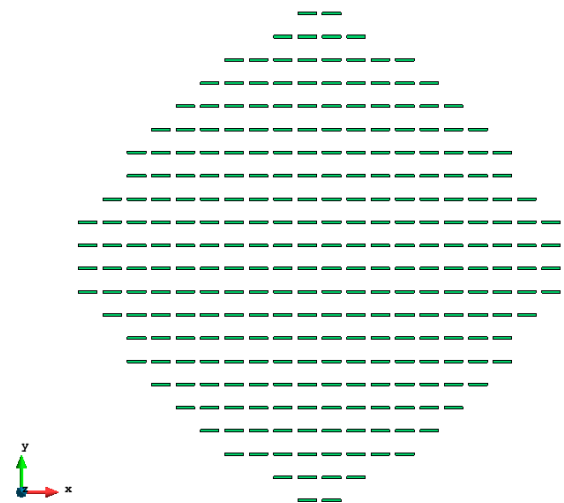

Fig. 1. Model of weather radar antenna

In the present paper two computational models are described. The first model is an improved Physical Optics approach that takes into account the wall thickness and multiple layers of the radome. The second model follows from the fast numerical solution of Electric and Magnetic Field Integral equations by means of the Multi-Level Fast Multipole Algorithm (MLFMA). This has been implemented in NLR in-house developed software and is also accessible in the commercially available FEKO software package of Altair. The improved Physical Optics model and both MLFMA approaches for the numerical solution of the Stratton-Chu integral equations are applied to a generic radome and radar antenna with properties similar to those of fighter aircraft. Differences in radiation patterns obtained by all three methods are discussed. Both NLR in-house tools are also applied to an available fighter-like radome and antenna.

II. MODELLING OF RADAR ANTENNA

The radar antenna modelled behind the generic radome is a slotted waveguide antenna. The electric field in a far-field point P originating from the entire antenna containing the 280 slots shown in Fig. 1 is modelled as in [1]:

$$\mathbf{E}_a(P) = \frac{\lambda}{\pi}\sin\left(\frac{\pi a}{\lambda}\right)\sum_{i=1}^{N_S}\left(-\frac{1+jkR_i}{R_i}w_i\hat{x}\times\hat{R}_i\right)\frac{e^{-jkR_i}}{4\pi R_i}, \quad (1)$$

in which k is the wavenumber and the wavelength λ equals 32mm. The dimensions of a single slot are a=18.8mm and b=2.7mm, N_S is the amount of slots in the antenna, $\hat{x}$ is the x-axis unit vector and finally:

$$R_i = \sqrt{(x_P - x_i)^2 + (y_P - y_i)^2 + (z_P)^2}$$

$$\hat{R}_i = 1/R_i \cdot [x_P - x_i \quad y_P - y_i \quad z_P]^T$$

$$w_i = \cos^2\left(\pi\sqrt{x_i^2 + y_i^2}\bigg/2R_0\right).$$
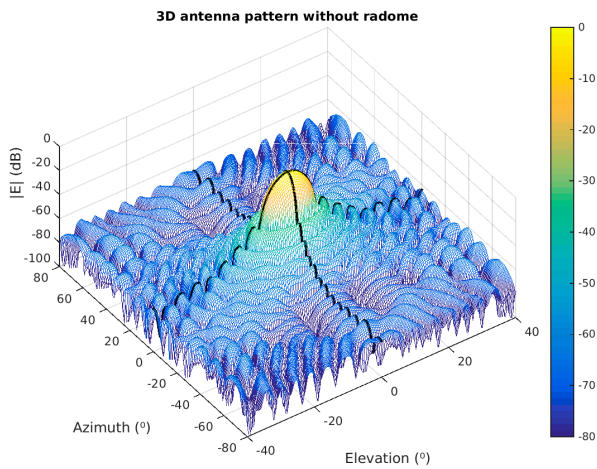

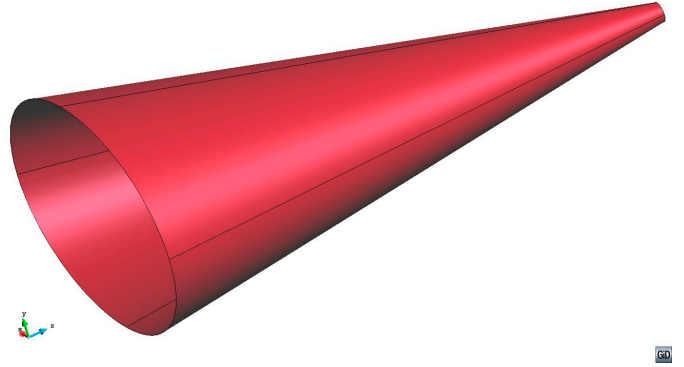Fig. 2. 3D far-field radiation pattern of the radar antenna in Fig. 1.

Fig. 3. CAD drawing of generic radome.

The tapering of the antenna is given by a weight w_i for each single slot. The total antenna field in (1) is therefore a weighted sum over the field originating from every slot. In the above (x_P, y_P, z_P) are coordinates of the point P and $(x_i, y_i, 0)$ are those of slot i. The antenna is centred in the origin of the coordinate centre and distances between adjacent slots in horizontal and vertical direction are dx=24.5 mm respectively dy=23.3 mm. Finally as typical radial dimension of the total antenna R_0 is taken to be 232.8 mm. The above model results in a scaled radiation pattern given in Fig. 2.

III. DESCRIPTION OF NOSE RADOME

For protection against weather, radar antennas are covered by radomes. For this paper a generic radome is designed which is shown in Fig. 3. It has dimensions equal to typical fighter aircraft. The length of this cone-like radome is 180cm and its basis is an ellipse with major radius 50cm and minor radius 35 cm. The tip is terminated with a small circle with radius 3 cm. This circular tip is shifted 15cm downwards with respect to the centre of the ellipse. As a consequence, the radome has only port starboard symmetry.

The dielectric radome has a thickness d of 7 mm, relative permittivity of ε_r =4 and a loss tangent $\tan\delta$ =0.025.

IV. SCATTERING OF RADOMES

The radar antenna illuminates the inside of the radome and induces electric and magnetic surface currents. These currents can be calculated in several ways, of which two are Physical Optics and Method of Moments. The following sections explain first an improved PO and then two accelerated MoM implementations.

A. Improved Physical Optics method

Physical Optics provides an approximation to the surface currents in terms of the transverse components of the EM fields. The method is accurate for bodies or surfaces that are large in terms of wavelengths. Since the designed radome has an area of about $2600\lambda^2$ this high-frequent approximation should be valid. The improved PO can be applied to dielectric

radomes with stratified walls and calculates currents on both interior reflected and outer transmitted surface of the dielectric radome, S_r and S_t. This is illustrated in Fig. 4, in which a multi-layered dielectric structure is illuminated by an incident field. This causes electric and magnetic surface currents $\mathbf{J}_r$, $\mathbf{M}_r$ and $\mathbf{J}_t$, $\mathbf{M}_t$ on the two indicated surfaces.

Besides having an electrically large dielectric structure, it is assumed that for a single slot the radome is in the far-field. Therefore, incident waves due to single slots can be approximated by plane waves. Moreover it is assumed that the curvature of the radome with respect to the sizes of the triangular mesh is small enough to represent a plane wave approaching a grid element by a wave approaching an infinite dielectric plane. In that case transmission and reflection coefficients $T_\perp$, $R_\perp$, $T_\parallel$, $R_\parallel$ (perpendicular and parallel to the plane of incidence) can be computed by a matrix method presented in [3]. An advantage is that this method enables calculating transmission and reflection through structures with multiple layers with different thickness, permittivity, permeability and conductivity.

Since the far-field assumption might hold for a single radiator and not the total antenna, currents on each grid element of the radome are calculated for each single slot. Total currents are obtained by a weighted sum of all these currents with weights equal to those in (1). Together with the normal of a triangular element the direction of an incident wave spans the incident plane. Incident electric fields are decomposed in a direction perpendicular and parallel to this plane, of which directional vectors are $\hat{d}_{\perp,i}$ and $\hat{d}_{\parallel,i}$ respectively. Define $\hat{k}_i$ as the direction of the incident plane wave. Since on both sides of the radome the medium is free space, the direction of the transmitted wave is equal to that of the incident wave. The direction of the reflected wave changes in normal direction:

$$\hat{k}_r = \hat{k}_i - 2\hat{n}_r\left(\hat{n}_r \bullet \hat{k}_i\right), \qquad \hat{k}_t = \hat{k}_i.$$

The normals on the inner and outer surfaces are denoted by $\hat{n}_r$ and $\hat{n}_t$ respectively. The direction vectors for transmitted end reflected field follow from:

$$\hat{d}_{\perp,r} = \hat{d}_{\perp,t} = \hat{d}_{\perp,i}, \hat{d}_{\parallel,t} = \hat{d}_{\parallel,i}, \hat{d}_{\parallel,r} = \hat{k}_r \times \hat{d}_{\perp,r}\Big/\left|\hat{k}_r \times \hat{d}_{\perp,r}\right|.$$

Then the transmitted and electric fields caused by the incident field of a single slot at the centre of a triangular element equal:

$$\mathbf{E}_t(\mathbf{r}) = \hat{d}_{\parallel,t}T_\parallel\left(\hat{d}_{\parallel,i}\bullet\mathbf{E}_i\right) + \hat{d}_{\perp,t}T_\perp\left(\hat{d}_{\perp,i}\bullet\mathbf{E}_i\right), \quad \mathbf{r} \in S_t,$$
$$\mathbf{E}_r(\mathbf{r}) = \hat{d}_{\parallel,r}R_\parallel\left(\hat{d}_{\parallel,i}\bullet\mathbf{E}_i\right) + \hat{d}_{\perp,r}R_\perp\left(\hat{d}_{\perp,i}\bullet\mathbf{E}_i\right), \quad \mathbf{r} \in S_r. \tag{2}$$

Given the plane wave assumption and the free space intrinsic impedance η the corresponding magnetic fields are given by:

$$\mathbf{H}_t(\mathbf{r}) = \hat{k}_t \times \mathbf{E}_t\Big/\eta, \qquad \mathbf{r} \in S_t,$$
$$\mathbf{H}_r(\mathbf{r}) = \hat{k}_r \times \mathbf{E}_r\Big/\eta, \qquad \mathbf{r} \in S_r, \tag{3}$$
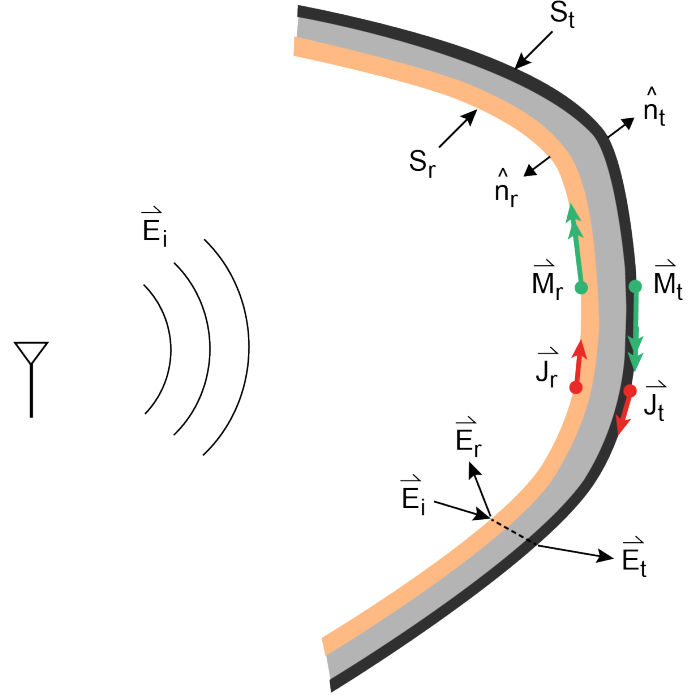

Fig. 4. Schematic overview of improved Physical Optics applied to a multi-layered structure. The method regards surface currents on the reflected and transmitted side of the dielectric body (subscripted by r respectively t).

The Physical Optics approximation provides the surface currents in the inner and outer surface of the radome, subscripted respectively by r and t:

$$\begin{aligned}
\mathbf{J}_t &= \hat{n}_t \times \mathbf{H}_t & \mathbf{r} &\in S_t \\
\mathbf{J}_r &= \hat{n}_r \times \left(\mathbf{H}_i + \mathbf{H}_r\right) & \mathbf{r} &\in S_r \\
\mathbf{M}_t &= \mathbf{E}_t \times \hat{n}_t & \mathbf{r} &\in S_t \\
\mathbf{M}_r &= \left(\mathbf{E}_i + \mathbf{E}_r\right) \times \hat{n}_r & \mathbf{r} &\in S_r.
\end{aligned} \tag{4}$$

The total surface currents on one grid element are obtained by applying a weighted sum over all antenna slots on the currents in (4). Once these total currents have been obtained the total electric field at a far-field point P can be found from:

$$\mathbf{E}_{total}(P) = \mathbf{E}_a(P) + \mathbf{E}_S(P), \tag{5}$$

in which the scattered electric field $\mathbf{E}_S$ is calculated from the surface currents by the Stratton-Chu formulation [2] applied to both the interior surface S_r and the outer surface S_t. An improvement to this formulation is found by calculating the surface integrals only on the reflected surface S_r. To this end a phase correction should be applied to the currents living on the outer surface, thereby projecting them on the inner surface. The magnitude of this phase correction is $kd\hat{n}_t \bullet \hat{r}_P$. Then the surface integration can be restricted to the inner surface S_r:

$$
\begin{aligned}
E_{s,\theta}\left(P\right) &= \nu\iint_{S_r}\left(\mathbf{J}_t e^{jkd\hat{n}_t\bullet\hat{r}_P}+\mathbf{J}_r\right)\bullet\hat{\theta}_P e^{jk\mathbf{r}'\bullet\hat{r}_P}dS' \\
&+ \iint_{S_r}\frac{1}{\eta}\left(\mathbf{M}_t e^{jkd\hat{n}_t\bullet\hat{r}_P}+\mathbf{M}_r\right)\bullet\hat{\phi}_P e^{jk\mathbf{r}'\bullet\hat{r}_P}dS' \\
E_{s,\phi}\left(P\right) &= \nu\iint_{S_r}\left(\mathbf{J}_t e^{jkd\hat{n}_t\bullet\hat{r}_P}+\mathbf{J}_r\right)\bullet\hat{\phi}_P e^{jk\mathbf{r}'\bullet\hat{r}_P}dS' \\
&- \iint_{S_r}\frac{1}{\eta}\left(\mathbf{M}_t e^{jkd\hat{n}_t\bullet\hat{r}_P}+\mathbf{M}_r\right)\bullet\hat{\theta}_P e^{jk\mathbf{r}'\bullet\hat{r}_P}dS'.
\end{aligned}
\tag{6}
$$

Here $\nu = -jk\eta e^{-jkr_P}\big/4\pi r_P$. By assuming constant currents on a single triangular element these equations are approximated by a sum over the entire radome mesh. In contrast to full-wave methods in the improved PO multiple reflections are not taken into account, nor is the attenuation when a first reflection again encounters the radome wall. However the developed method allows for computational analysis of stratified radomes in a matter of an hour, even on a simple laptop.

B. Full-wave methods

A more exact numerical method to obtain the desired surface currents is the full-wave Method of Moments. This section briefly describes the most important features of two implementations of this full-wave method for homogeneous dielectric bodies. One of the implementations is the fast-multipole-accelerated Methods-of-Moments algorithm in the commercially available FEKO software package of Altair [4]. The other implementation is the NLR in-house developed code Shako. Both implementations solve Methods of Moments discretisations of boundary integral equations for dielectric bodies and accelerate the solution process by a multi-level fast multipole algorithm (MLFMA, see [9], for instance).

There are several formulations for boundary integral equations of the scattering from homogeneous dielectric bodies. Most popular are the Poggio, Miller, Chang, Harrington, Wu (PMCHW(T)) [6] and Müller [7] formulations. FEKO uses the PMCHW formulation, which is discretised using the standard Rao-Wilton-Glisson (RWG) test and basis functions [10]. Shako uses the Müller formulation, discretised using RWG basis functions and Buffa-Christiansen (BC) test functions [11], as first introduced by [8]. Broadly speaking the PMCHW formulation has comparable characteristics to EFIE for PEC and the Müller formulation comparable to MFIE. The use of the BC test functions improves the accuracy of the Müller formulation [8].Finally, both solvers use double-precision arithmetic.

Similar to PO, after the current distribution over the radome surface has been obtained, far-field equations lead to the corresponding scattered field. Total electric fields are again obtained by (5). These full-wave methods then accurately describe the exact behaviour of radome and antenna including all interactions, though for both Shako and FEKO at the expenses of large computational resources (example: 4.6 hours on 16 cores and 138GB RAM for FEKO).
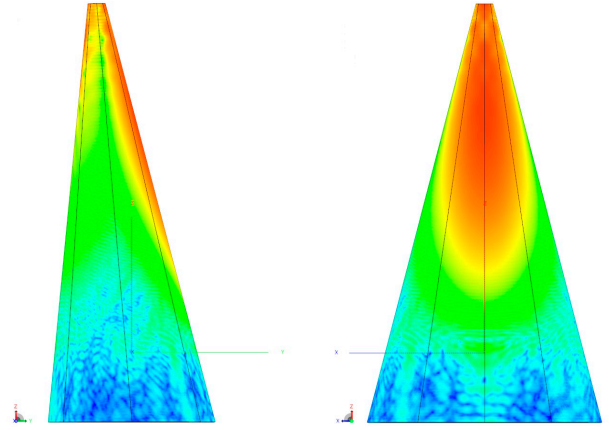

Fig. 5. Side- and topview of electrical surface currents (dBA/m) on the generic radome obtained by FEKO.

TABLE I.   IMPORTANT PROPERTIES OF THE MAIN BEAM FOR GENERIC RADOME AND ANTENNA, COMPUTED BY THREE DIFFERENT METHODS

Code	Main beam property		
	Attenuation	Deflection – Elevation	Deflection – Azimuth
NLR- PO	-2.68 dB	1.67°	0°
NLR -Shako	-1.45 dB	1.50°	0°
FEKO	-2.11 dB	1.60°	0°

V. RESULTS OF SIMULATIONS

A. Generic Radome

By applying the introduced methods of section IV to the generic radome and antenna electric and magnetic surface currents are obtained. An example of the electric currents computed by FEKO is shown in Fig. 5. Effects of for instance multiple reflections can be observed, especially in the area of the nose.

After applying far-field equations like (6) for all three obtained current solutions radiation patterns are obtained, of which horizontal and vertical cross sections are given in 0. It shows a very good comparison between the two full-wave methods. The PO method in general also coincides well, although evidently there are some differences. All codes show a clear image lobe caused by the reflection of the main lobe and the positions of these reflections coincide up to a few degrees. The level of the image lobe for PO is 1-2dB higher than those computed by Shako and FEKO. This is since the current PO solver lacks attenuation when the first reflection hits the other side of the radome. Moreover it only takes into account one reflection, which explains the difference in levels for magnitudes of azimuth larger than 50 degrees. MoM obtains a second reflection in these regions, while PO obtains a significantly smaller electric field.

Apart from the image lobe important features of the radiation pattern concern the main lobe. The values of these properties obtained by all three codes are given in TABLE I.
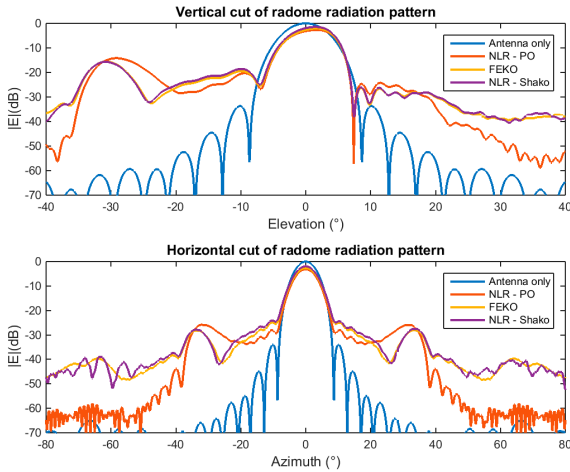
Fig. 6. Vertical and horizontal cross sections of the radiation patterns of the generic radome and radar antenna, obtained by the NLR in-house PO (red) and MoM (purple) codes and FEKO (yellow). Radar only given in blue.

There is a very good comparison between deflection angles in both directions for all codes. The attenuation of PO and FEKO differ only 0.57dB. For this property difference between FEKO and Shako of 0.66dB is a little larger.

B. Fighter-like radome

For a second benchmark NLR has the availability over a CAD-drawing of a fighter-like radome. This radome has dimensions similar to those of the generic radome in Fig. 3. For this computation the radome is modelled with a single layer that has electrical properties that are also comparable with the generic radome. Cross sectional radiation patterns for Shako and NLR – PO are given in Fig. 7. The orientation of the antenna was changed to an elevation of -14° and an azimuth of -16°. Since this causes fewer reflections than when aiming to the nose, this figure shows even better comparison between the full-wave Shako and the high-frequent PO. In this case the differences in main beam deflection are about 0.2°, but the directions of the deflection are equal.

VI. CONCLUSIONS

Two computational methods to analyse the effects of protective nose radomes on radar antennas are presented. The methods are applied to a generic radome and a fighter-like radome with slotted array antennas. Results of two implementations of full-wave Method of Moments are compared to an improved Physical Optics method. The latter takes into account wall thickness and can moreover be applied to multi-layered structures with different material properties. Comparison of radiation patterns shows a good match between results of the three methods. Especially important properties like main beam attenuation and deflection are estimated quite accurately. Differences appear because of a lack of multiple reflections and attenuation of the first reflection in the current NLR in-house PO solver. This causes for a slight overestimation of image lobe levels.

The full-wave solvers are more accurate. On the other hand results were obtained by PO on a simple laptop within reasonable amount of time, whereas the full-wave solvers require large computational resources. When high accuracy throughout the entire radiation pattern is desired, a full-wave solver should be preferred. For successive simulations when used for assistance in tuning a radome a fast solver like the improved PO is very useful.
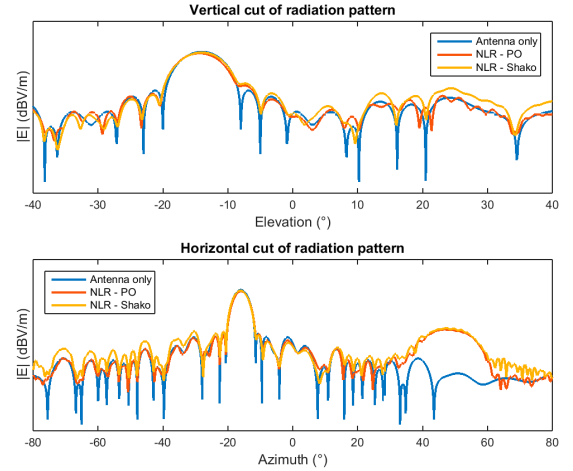

Fig. 7. Vertical and horizontal cross sections of the radiation patterns for a fighter-like antenna (blue). Results including radome as obtained by the NLR in-house PO (red) and MoM (yellow) codes. Scales are removed on request.

REFERENCES

[1] A. Piche, G.P. Piau, C. Bernus, F. Campagna and D. Balitrand, "Prediction by simulation of electromagnetic impact of radome on typical aircraft antenna", Antennas and Propagation (EuCAP), 2014 European Conference on, The Hague, pp. 3205-3208.

[2] David C. Jenn, "Radar and laser cross section engineering", American Institute of Aeronautics and Astronautics Inc., 1995.

[3] H. Oraizi and M. Afsahi, "Analysis of planar dielectric multilayers as FSS by transmission line transfer matrix method (TLTMM)", Progress In Electromagnetic Research, Vol. 74, pp. 217-240, 2007.

[4] Altair Development S.A. (Pty) Ltd, "FEKO http://www.altairhyperworks.com/Product,73,FEKO.aspx)"

[5] H. van der Ven and H. Schippers, Mathematical definition document for the multilevel fast multipole method, Technical Report NLR-CR-2010-529, 2015.

[6] J. Mautz and R. Harrington, "Electromagnetic scattering from a homogenenous body of revolution," Department of Electrical and ComputerEngineering, Syracuse University, Technical Report TR-77-10, 1979.

[7] C. Müller, Foundations of the Mathematical Theory of Electromagnetic Waves. Springer, 1969.

[8] S. Yan, J.-M. Jin, and Z. Nie, "Improving the accuracy of the second kind Fredholm integral equations by using the Buffa-Christiansen functions," IEEE Trans. Ant. Prop., vol. 59(4), pp. 1299–1310, 2011.

[9] Weng Cho Chew, Jian-Ming Jin, Eric Michielssen, and Jiming Song. Fast and efficient algorithms in computational electromagnetics. Artech House, 2001.

[10] Sadavisa M. Rao, Donald R. Wilton, and Allen W. Glisson. Electromagnetic scattering by surfaces of arbitrary shape. IEEE Trans. Antennas and Propagat., 30(3):409–418, 1982.

[11] A. Buffa and S.H. Christiansen. A dual finite element complex on the barycentric refinement. Math. Comput., 260:1743–1769, 2007.

This page is intentionally left blank.